Phase-Controlled Beamforming Network Intended for Conformal Arrays

Valentina Palazzi

Department of Engineering
University of Perugia
Perugia, Italy
E-mail: valentina.palazzi@unipg.it

Abstract

This work describes a reconfigurable 1 × 4 network able to provide beamforming capabilities to conformal antenna arrays. In particular, the proposed feed network is able to activate either single output ports or couples of adjacent output ports of a four-element array. The output-port selection is achieved by controlling only the phase of four variable phase shifters. In the case where two output ports are activated, the network is also able to control the phase relationship between the signals, enabling in-phase and 180°-out-of-phase signal configurations. To test the developed theory, a prototype in microstrip technology, designed to operate in the recently released sub-6 GHz 5G 3.4 GHz to 3.8 GHz band, was manufactured, confirming adequate behavior of the network. The proposed circuit was then connected to a four-element antenna cube where it was used to generate twelve different beams: eight equally-spaced beams over 360° with maximum gain in their broadside direction, which enabled a uniform coverage of the azimuthal plane, and four equally-spaced beams with nulls in their broadside direction, useful in applications such as interference removal and radio localization.

1. Introduction

As the number of wireless connected devices rapidly increases, the resources of current telecommunication systems are sufficient to meet all traffic needs [1-3]. A shortage of available frequency bands and interference issues may cause trouble for communications, thereby threatening connection reliability. To solve these issues and to improve the capacity of the network, upcoming communication standards are being designed to include countermeasures, such as new broader transmission bands and beamforming capabilities.

Since most of the upcoming 5G systems, including base stations, handheld devices, and hotspots, will be equipped with beam-steering and beamforming techniques, an impending need for reconfigurable transponders has emerged [4]. Such techniques allow front-ends to transmit a given signal only toward the desired recipients, reducing both interference and the transmitted power needed for a given transmission range [5]. Broadband microwave components are also being developed to take advantage of the new released bands and to guarantee higher transmission speeds.

Well-known beamforming-circuit configurations, such as the Butler matrix, are attracting renewed attention [6, 7]. However, most of the available studies were intended for linear arrays with an angular coverage lower than 180°, while complex multilayer topologies are required to achieve spatial scanning [8, 9]. At the same time, research is also focusing on reconfigurable power dividers, which can be used, among other things, to perform beamforming for conformal arrays [10-12].

This work describes the design, the theoretical analysis, and the experimental validation of a feed network intended for antenna topologies with radiating elements placed on the lateral sides of polygons (square in the specific case). The network is able to guarantee homogeneous 360° beam-steering in the azimuthal plane, while keeping control of the shape of the generated radiation patterns. This feed network was firstly presented in [13]. Here, the circuit is theoretically analyzed and tested in a more comprehensive way. The circuit design is described in Section 2, while the performance and experimental results of the fabricated prototype are discussed in Section 3.

2. Circuit Design

Figure 1 shows a conformal array composed of four radiating elements placed on the lateral sides of a cube and oriented according to the cardinal directions, i.e., north (N), east (E), south (S), and west (W), where the distance among radiating elements is lower than one wavelength in their operating band. When the antennas are individually fed, their radiation patterns have a maximum in the respective broadside directions (see radiation patterns N, S, E, W in Figure 1a). Moreover, additional radiation patterns are obtained when couples of adjacent radiating elements are simultaneously fed, with the following characteristics:

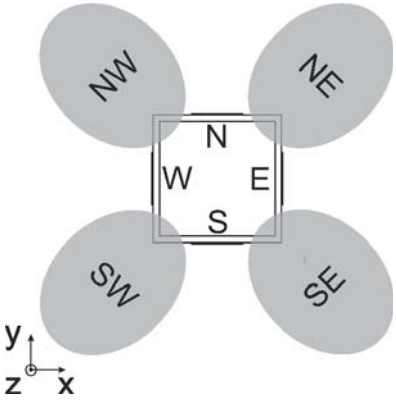

Figure 1a. A sketch of the proposed antenna system: radiation patterns (in gray) generated by single radiating elements. The four radiating elements are marked with their corresponding cardinal directions: N, E, S, and W.

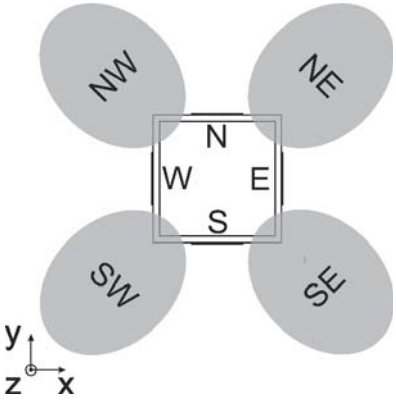

Figure 1b. A sketch of the proposed antenna system: radiation patterns generated by couples of radiating elements fed with in-phase equal-magnitude signals.

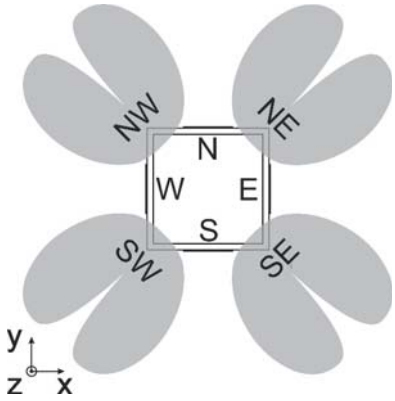

Figure 1c. A sketch of the proposed antenna system: radiation patterns generated by couples of radiating elements fed with 180° out-of-phase equal-magnitude signals.

- In the case where adjacent couples are excited with in-phase equal-magnitude signals, radiation patterns with maxima in the intermediate directions NE, SE, SW, and NW and antenna gains and beamwidths almost similar to the single radiating elements are obtained (see Figure 1b);

- In the case where adjacent antennas are fed with 180° out-of-phase signals, radiation patterns with nulls in the directions NE, SE, SW, and NW are obtained (see Figure 1c).

The first type of radiation patterns can be used to pursue a more homogeneous coverage of the azimuthal plane. Indeed, the H-plane 3-dB beamwidth of common radiating elements, such as patch antennas, is usually lower than 90°. This means that the gain of single antennas in the intermediate directions between adjacent radiating elements is lower than their maximum gain by more than 3 dB. Feeding both single antennas and couples of adjacent antennas with in-phase equal-magnitude signals, the number of steerable directions is doubled (from four to eight), thereby achieving a more homogeneous coverage without increasing the number of radiating elements of the array.

The second type of radiation patterns with a zero in the broadside direction (that can be obtained by feeding couples of adjacent radiating elements with equal-magnitude 180° out-of-phase signals) can profitably be used in many application scenarios, including interference removal in radio receivers (i.e., the zero can be oriented in the direction of the interference) and radio localization (i.e., the zero can be used to finely estimate the direction of arrival of a given radio signal). These additional features broaden the scope of the proposed array and improve its reliability.

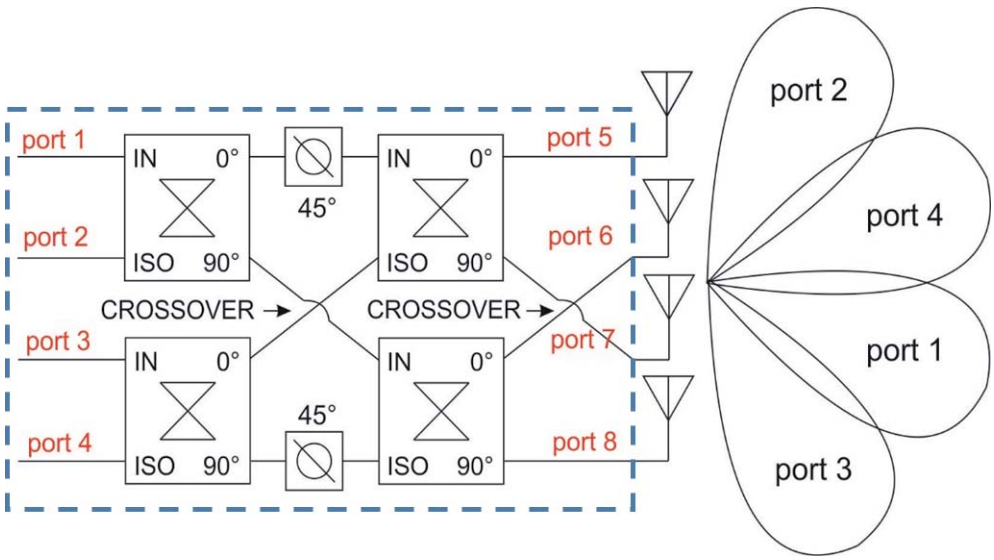

Figure 2. A schematic of a 4 × 4 Butler matrix.

Table 1. The 4 × 4 Butler matrix: relative phase difference among output ports as a function of activated input port.

Activated Input Port y	$\angle S_{x,y} - \angle S_{x+1,y}$ for $x = 5,...,8$
1	–45°
2	135°
3	–135°
4	45°

The goal of this paper is to develop a reconfigurable feed network for such a conformal array that is able to switch among the following states:

- Feed all single radiating elements;
- Feed all couples of adjacent radiating elements with equal-magnitude in-phase signals;
- Feed all couples of adjacent radiating elements with equal-magnitude 180° out-of-phase signals.

Traditional approaches, based on feed networks equipped with RF switches, are not applicable in this case, since each radiating element must be fed either individually or coupled to different adjacent elements without spoiling the matching conditions of the other elements, and this would lead to very tangled networks. We therefore decided to adopt an original approach, inspired by the Butler matrix topology [14]. The Butler matrix is an $N \times N$ circuit used to implement beam-steering (by way of example, Figure 2 shows the scheme of the 4 × 4 Butler matrix). Its working principle is as follows: one of the N input ports is selected and activated; the input power is equally divided by the network among the N output ports, and a constant phase difference is imposed among adjacent ports, where the latter difference varies with the selected input port (Table 1 reports the phase differences corresponding to the activated input ports for the 4 × 4 network).

Since the matrix is reciprocal, its output ports can be logically exchanged with the input ports. This means that if we feed all input ports using signals with equal magnitude and specific phase differences, the input power can be combined toward a single output port (the activated output port depends on the selected phase differences). In the present work, we investigated whether we could modify the Butler-matrix architecture and find phase relations among the input signals so that we could combine the input power not only toward single output ports, but also toward couples of adjacent output ports.

The scheme of the proposed feed network (patent pending) is shown in Figure 3. The input signal at port 1 is divided into four equal parts by a four-way power divider. Each signal is then phase shifted by a variable phase shifter (the phase variables are marked with the Greek letters α, β, γ and δ). Finally, the obtained signals enter the 4 × 4 matrix, so that the desired output ports are activated. The matrix is composed of four 90° hybrid couplers like the 4 × 4 Butler matrix, while the two 45° phase shifters are replaced by two 90° phase shifters.

Assuming all components and interconnections are ideal, the S-parameter matrix of the network can be easily calculated as follows:

$$[S] = \begin{bmatrix} 0 & S_{21} & S_{31} & S_{41} & S_{51} \\ S_{21} & 0 & 0 & 0 & 0 \\ S_{31} & 0 & 0 & 0 & 0 \\ S_{41} & 0 & 0 & 0 & 0 \\ S_{51} & 0 & 0 & 0 & 0 \end{bmatrix}$$

The transmission coefficients of the network S_{k1}, where $k = 2,...,5$, are composed of four terms that combine to determine the selected output signals of the network based on the values of the phase variables α, β, γ, and δ, as follows:

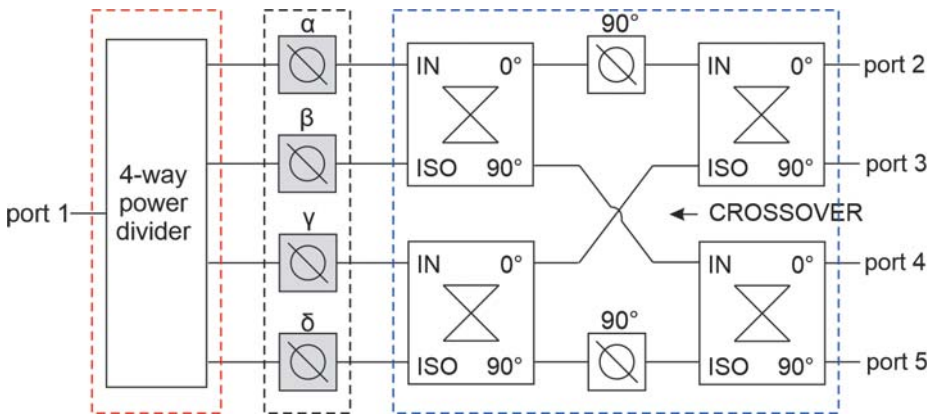

Figure 3. A schematic of the proposed 1 × 4 reconfigurable feed network.

$$S_{21} = \frac{1}{4}\left(-je^{-j\alpha} - e^{-j\beta} - je^{-j\gamma} - e^{-j\delta}\right), \quad (1)$$

$$S_{31} = \frac{1}{4}\left(-e^{-j\alpha} + je^{-j\beta} + e^{-j\gamma} - je^{-j\delta}\right), \quad (2)$$

$$S_{41} = \frac{1}{4}\left(-je^{-j\alpha} + e^{-j\beta} + je^{-j\gamma} - e^{-j\delta}\right), \quad (3)$$

$$S_{51} = \frac{1}{4}\left(-e^{-j\alpha} - je^{-j\beta} - e^{-j\gamma} - je^{-j\delta}\right). \quad (4)$$

From Equations (1)-(4), the squared magnitudes of the transmission coefficients can be expressed as follows:

$$|S_{21}|^2 = \frac{1}{4} + \frac{1}{8}(a+b), \quad (5)$$

$$|S_{31}|^2 = \frac{1}{4} + \frac{1}{8}(a-b), \quad (6)$$

$$|S_{41}|^2 = \frac{1}{4} + \frac{1}{8}(-a+c), \quad (7)$$

$$|S_{51}|^2 = \frac{1}{4} + \frac{1}{8}(-a-c), \quad (8)$$

where auxiliary variables are introduced to simplify the analysis:

$$a = \sin(x) + \sin(y), \quad (9)$$

$$b = \cos(z) + \sin(z+y) - \sin(z-x) + \cos(z+y-x) \quad (10$$

$$c = -\cos(z) + \sin(z+y) - \sin(z-x) - \cos(z+y-x) \quad (11)$$

$$x = \alpha - \beta, \quad (12)$$

$$y = \gamma - \delta, \quad (13)$$

$$z = \alpha - \gamma. \quad (14)$$

The phases of the transmission coefficients can be expressed as functions of x, y, and z as follows:

$$\angle S_{21} = \tan^{-1}\left[\frac{-\cos(\alpha) + \sin(\alpha - x) - \cos(\alpha - z) + \sin(\alpha - z - y)}{-\sin(\alpha) - \cos(\alpha - x) - \sin(\alpha - z) - \cos(\alpha - z - y)}\right] \quad (15)$$

$$\angle S_{31} = \tan^{-1}\left[\frac{\sin(\alpha) + \cos(\alpha - x) - \sin(\alpha - z) - \cos(\alpha - z - y)}{-\cos(\alpha) + \sin(\alpha - x) + \cos(\alpha - z) - \sin(\alpha - z - y)}\right] \quad (16)$$

Table 2. The relationships among output signal configurations and auxiliary variables.

$\|S_{21}\|^2$	$\|S_{31}\|^2$	$\|S_{41}\|^2$	$\|S_{51}\|^2$	a	b	c	x	y	z	**Phase Diff.**
1	0	0	0	2	4	0	90°	90°	0°	/
0	1	0	0	2	–4	0	90°	90°	180°	/
0	0	1	0	–2	0	4	270°	270°	180°	/
0	0	0	1	–2	0	–4	270°	270°	0°	/
½	½	0	0	2	0	0	90°	90°	270° 90°	0° 180°
0	0	½	½	–2	0	0	270°	270°	90° 270°	0° 180°
½	0	0	½	0	2	–2	180° 0°	180° 0°	0°	0° 180°
0	½	½	0	0	–2	2	0° 180°	0° 180°	180°	0° 180°

$\angle S_{41} =$

$$\tan^{-1}\left[\frac{-\cos(\alpha)-\sin(\alpha-x)+\cos(\alpha-z)+\sin(\alpha-z-y)}{-\sin(\alpha)+\cos(\alpha-x)+\sin(\alpha-z)-\cos(\alpha-z-y)}\right] \quad (17)$$

$\angle S_{51} =$

$$\tan^{-1}\left[\frac{\sin(\alpha)-\cos(\alpha-x)+\sin(\alpha-z)-\cos(\alpha-z-y)}{-\cos(\alpha)-\sin(\alpha-x)-\cos(\alpha-z)-\sin(\alpha-z-y)}\right] \quad (18)$$

We therefore first determine the auxiliary variables *a*, *b*, and *c*, corresponding to the magnitude configurations of interest, according to Equation (5)-(8). We then find the corresponding values of *x*, *y*, and *z*. We finally obtain the phase relationships between the activated signals according to Equations (15)-(18).

The results are shown in Table 2. In cases corresponding to one-port activations (i.e., the first four cases in Table 2), a unique solution for *x*, *y*, and *z* is obtained for each triplet *a*, *b*, and *c*. On the other hand, in cases corresponding to two-port activations, two *x*, *y*, and *z* solutions are found for each triplet *a*, *b*, and *c*: one corresponding to in-phase output signals and the other to 180° out-of-phase signals. It is worth mentioning that since the network is intended to be utilized in circular arrays, port 2 is considered to be adjacent to port 5.

The last step is to determine the phase variables α, β, γ, and δ, corresponding to the auxiliary variables *x*, *y*, and *z*. To do so, we need to solve the system of Equations (12)-(14) comprised of three linear equations with four unknowns. Such a system has infinite solutions: this means that the value of one of the four phase shifters can be arbitrarily set, and that multiple phase combinations can lead to the same output signal configuration.

One representative phase solution is reported in Table 3 for each output signal configuration. All phase variables were multiples of 90°. Therefore, they could be implemented using two-bit phase shifters. A progressive number, *N*, was associated with each phase configuration for future reference.

The final system presented one RF input port, four RF output ports, and the relevant control pins for the variable phase shifters. The proposed feed network not only made it possible to activate couples of adjacent output ports with in-phase signals (see rows for $N = 5,...,8$ in Table 3), but also with 180° out-of-phase signals (see rows for $N = 9,...,12$ in Table 3). It therefore provided the system with additional beamforming capabilities that will further improve the system's ability to be reconfigured and its field of applications.

3. Experimental Results

A prototype of the proposed feed network in microstrip technology was designed, manufactured, and tested (see Figure 4). The main parts of the circuit were surrounded by three rectangles, corresponding to those shown in Figure 3:

- A fixed four-way power divider (red rectangle), composed of three cascaded two-way Wilkinson dividers;
- A bank of four variable phase shifters (black rectangle): each block consisted of a two-bit switched-line phase shifter. Commercial voltage-controlled single-pole double-through switches (AS179-92LF model from Skyworks [15]) were used to select the desired path. Each switch introduced an insertion loss of 0.5 dB, thereby leading to an overall phase-shifter insertion loss of about 2 dB. The control pins of the switches were connected to the power supply through wires.

Table 3. The relationships among phase variables and activated output ports.

N	α	β	γ	δ	Output Ports	Phase Diff.
1	90°	0°	90°	0°	2	/
2	90°	0°	270°	180°	3	/
3	180°	270°	0°	90°	4	/
4	0°	90°	0°	90°	5	/
5	90°	0°	180°	90°	2-3	0°
6	0°	180°	180°	0°	3-4	0°
7	90°	180°	0°	90°	4-5	0°
8	0°	0°	0°	0°	2-5	0°
9	180°	90°	90°	0°	2-3	180°
10	0°	0°	180°	180°	3-4	180°
11	0°	90°	90°	180°	4-5	180°
12	0°	180°	0°	180°	2-5	180°

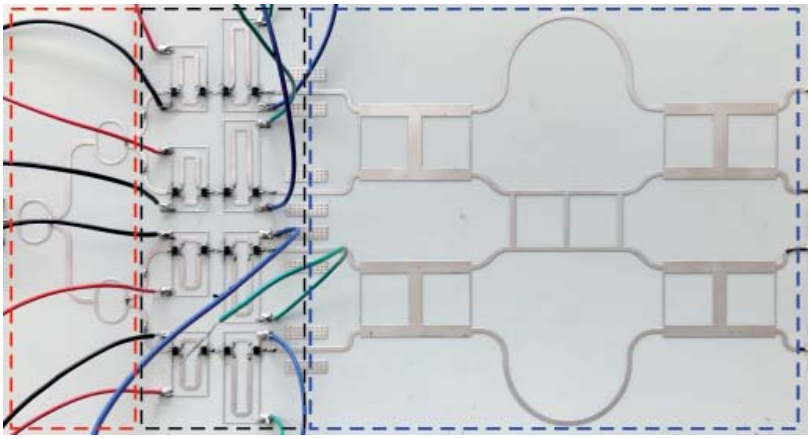

Figure 4. The prototype of the complete feed network: (l-r) four-way power divider (red rectangle), two-bit phase shifters (black rectangle) and 4 × 4 matrix (blue rectangle). The visible wires are for switching control. The active area was 20 cm² × 10 cm² (after [13]).

- A Butler-like 4 × 4 matrix (blue rectangle): the four 90° hybrid couplers and the crossover of the matrix were implemented with "double-box" 3 dB and 0 dB branch-line couplers, respectively. The "double-box" configuration was chosen to improve the operating bandwidth of the system. The two 90° fixed phase shifters were implemented with quarter-wave line sections.

The prototype was designed to operate in the sub-6 GHz 5G band (3.4 GHz to 3.8 GHz: i.e., 11% bandwidth around 3.6 GHz), and the substrate adopted was 0.5-mm-thick Roger 4350B substrate ($\varepsilon_r = 3.66$, $\tan\delta = 0.004$).

The three parts of the circuit were first separately studied. The four-way power divider and the bank of phase shifters were designed by performing schematic simulations within *Advanced Design Suite* (*ADS*), while full-wave simulations were used for the Butler-like 4 x 4 matrix (the FEM simulator of *CST Studio Suite* was used). Finally, the *S* parameters of the latter part were imported within *ADS* and the whole circuit was simulated (co-simulation approach).

The *S* parameters of the manufactured feed-network prototype were measured with a vector network analyzer (VNA, FieldFox N9981A model). The transmission coefficients obtained for the output signal configurations of interest are shown in Figure 5-7 and compared to simulation results. A good agreement was observed in all cases.

Figure 5 shows the magnitude of the transmission coefficients in the single-port activation configurations, i.e., for $N = 1,..,4$. The magnitude of the transmission coefficients of the activated ports was around -3.7 dB in all four cases, accounting for both the insertion loss of the switches (around 2 dB) and the line loss (which resulted in about 1.7 dB). It was significantly flat in all the band of interest, with a very small maximum variation of 0.5 dB. The transmission coefficients of the deactivated ports were below -19 dB.

On the other hand, the magnitude of the transmission coefficients of the activated ports in the two-port activation configurations with in-phase signals was around 3 dB below the single-port configurations. This was due to the fact that the input power was split between two ports, as shown in Figures 6a and 6c. A still satisfactory maximum

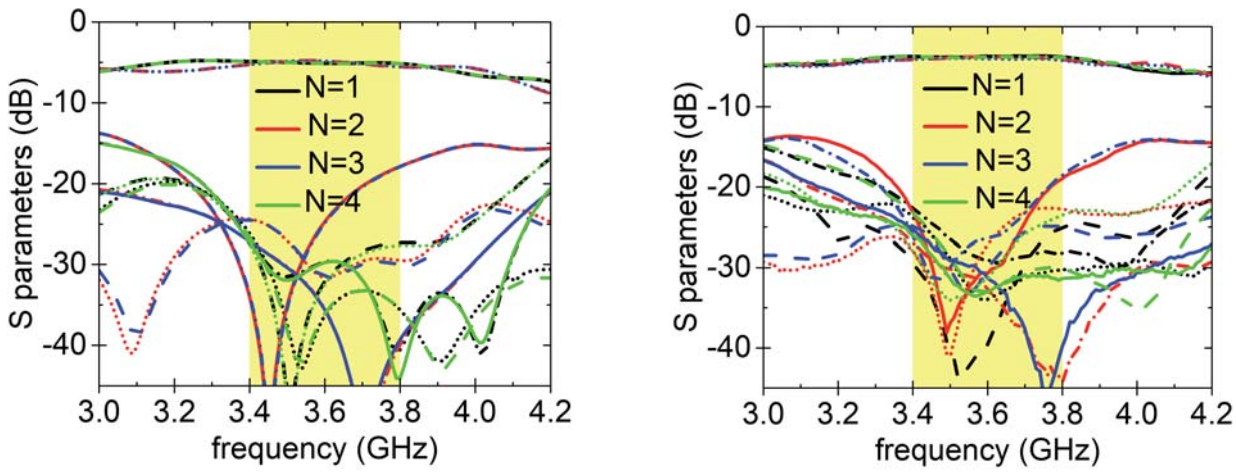

Figure 5. The simulated (a) and measured (b) magnitudes of the transmission coefficients of the complete 1 × 4 network as functions of frequency for single-port activation. The solid line refers to $|S_{21}|$, the dashed line to $|S_{31}|$ the dotted line to $|S_{41}|$, and the dashed dotted line to $|S_{51}|$ (after [13]).

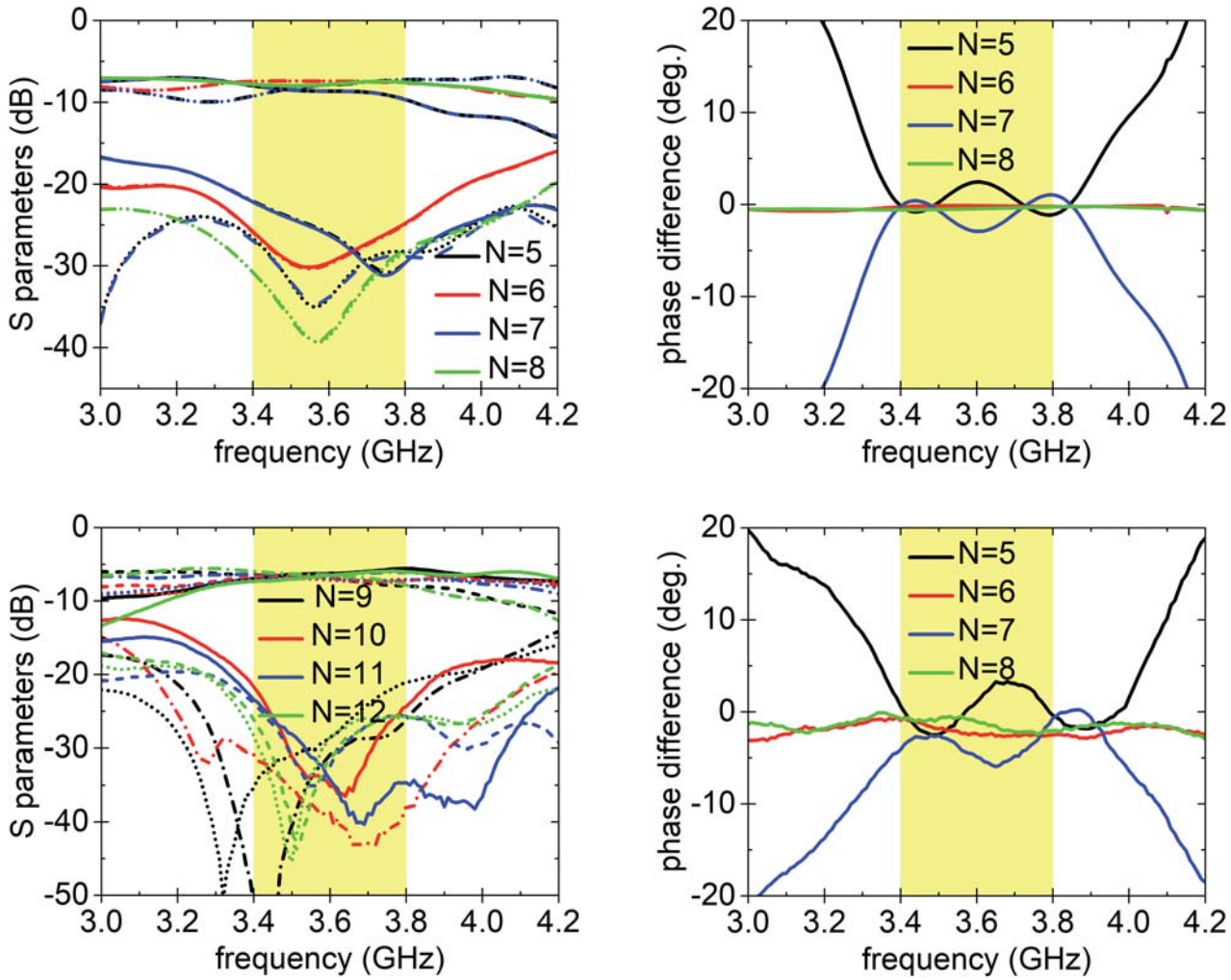

Figure 6. The magnitudes (a)-(c) and phase differences (b)-(d) of the transmission coefficients of the complete 1 × 4 network as functions of frequency for the cases $N = 5,...,8$. Plots (a)-(b) report simulation results and (c)-(d) show measurements. The solid line refers to $|S_{21}|$, the dashed line to $|S_{31}|$, the dotted line to $|S_{41}|$, and the dashed dotted line to $|S_{51}|$ (after [13]).

variation of less than 2 dB (i.e., transmission coefficient between -6.1 dB and -8 dB) was experienced in the band of interest. The transmission coefficients of the deactivated ports were below -24 dB.

Figures 6b and 6d illustrate the phase difference between the transmission coefficient of adjacent ports for cases $N = 5,...,8$. The measured phase differences between the two activated ports, ideally in phase, were below 6° in all cases in the whole band.

Finally, the magnitudes and phase differences of the transmission coefficients for $N = 9,...,12$ are shown in Figure 7. The magnitudes of the activated ports were on the same level as the in-phase cases shown in Figure 6, with a maximum variation lower than 2.2 dB in all the band. The transmission coefficients of the deactivated ports were below -21 dB. Concerning phase relationships, the signals corresponding to each couple of activated output ports were 180° out of phase, with a phase error lower that 8° in the band of interest.

Finally, an experiment was performed in a laboratory room to assess the beamforming capabilities of the designed network, as shown in Figure 8. Four square patch antennas, arranged on the sides of a cube, were designed and manufactured by using a 1.6 mm-thick low-cost FR4 substrate ($\varepsilon_r = 4.7$, $\tan\delta = 0.011$), to implement the antenna topology illustrated in Figure 1. The four patch antennas, placed on a rotating platform, were connected to the output ports of the proposed feed network by means of four identical flexible coaxial cables, while the input port of the feed network was connected to a vector network analyzer. The second port of the vector network analyzer was connected to a single patch antenna (right side of Figure 8). Both the single patch and the antenna cube were aligned and placed at a distance of 50 cm, so that they operated in their far-field regions.

The H-plane radiation patterns of the cube corresponding to the signal configurations of interest were finally evaluated (see Figures 9-11). The measurements were performed in an open-air environment without special

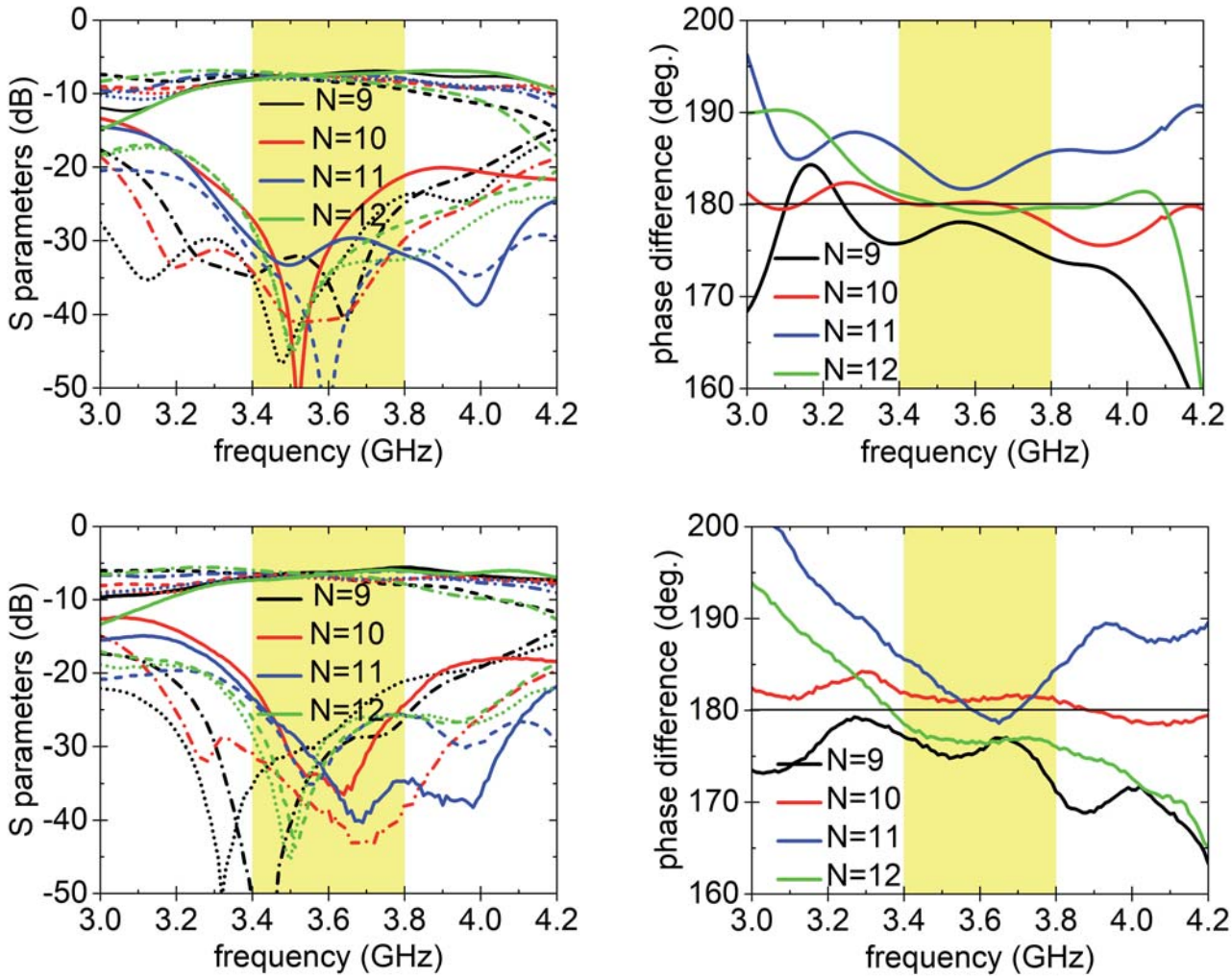

Figure 7. The magnitudes (a)-(c) and phase differences (b)-(d) of the transmission coefficients of the complete 1 × 4 network as functions of frequency for the cases $N = 9,...,12$. Plots (a)-(b) report simulation results and (c)-(d) show measurements. The solid line refers to $|S_{21}|$, the dashed line to $|S_{31}|$, the dotted line to $|S_{41}|$, and the dashed dotted line to $|S_{51}|$.

anechoic provisions, and were compared to the simulation results. Despite the impact of the measurement setup, there was a good agreement with the simulations, thus confirming the adequate behavior of the system. The absolute level of the received power along the directions of the maxima was fairly independent of the selected configuration (maximum measured difference below 1.1 dB among all cases).

In Figure 12, a comparison between the radiation patterns obtained with the signal configurations $N = 6$

Figure 8. A photo of the complete system, including the antenna topology and the beamforming network. The side of the cube was 45 mm, while the side of the square patch was 19.3 mm.

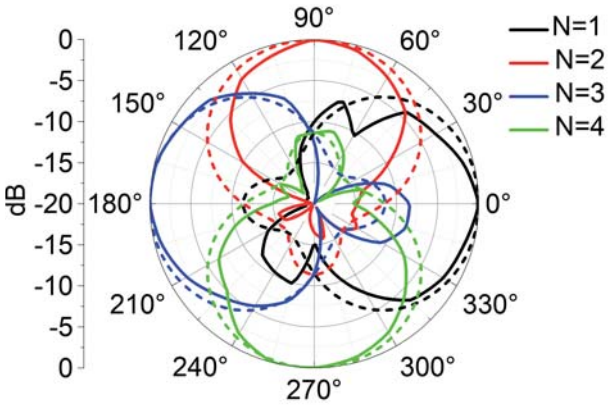

Figure 9. A comparison between simulated (dashed) and measured (solid) H_θ -plane (xy-plane) radiation patterns as a function of phase configurations. The input phases were configured for single-port activation (after [13]).

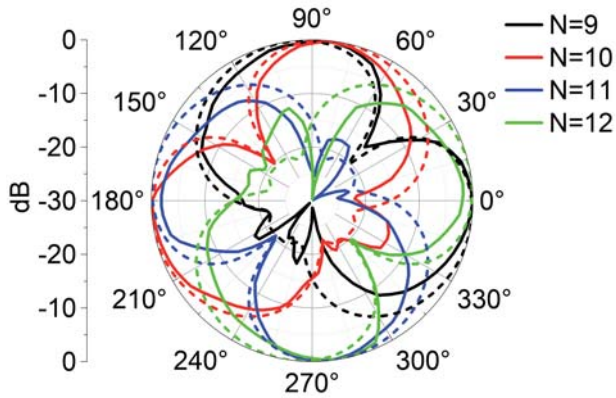

Figure 11. A comparison between simulated (dashed) and measured (solid) H_θ -plane (xy-plane) radiation patterns as a function of phase configurations. The input phases were configured for 180° out-of-phase two-port activation (after [13]).

and $N = 10$ are shown, corresponding to the cases where the same two output ports were activated (i.e., ports 3 and 4), either in-phase or 180° out of phase. For $N = 10$ a null was obtained, corresponding to the direction of maximum radiation for $N = 6$: the gain of the antenna in the broadside direction for $N = 10$ was more than 20 dB lower than the gain obtained for $N = 6$. This suggested that the feed network provided the antenna with additional beamforming capabilities that could be useful in many applications, such as, for instance, radio localization.

4. Conclusion

A phase-controlled 1 × 4 beamforming network for conformal arrays, able to feed either single antennas or a couple of adjacent radiating elements simultaneously, was described and theoretically analyzed. A single-layer feed-network prototype was fabricated, operating in the frequency range 3.4 GHz to 3.8 GHz, and featuring satisfactory performance throughout the band of interest. The feed network was connected to a four-element antenna

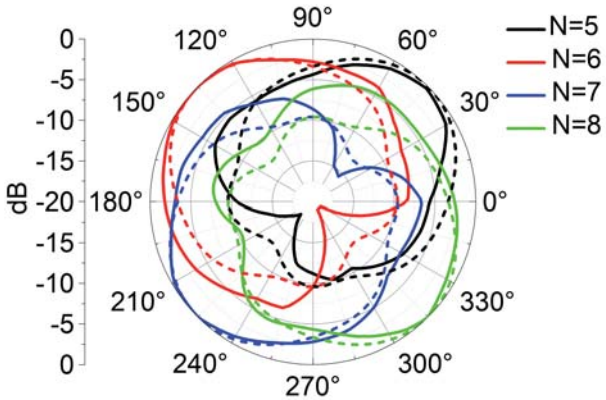

Figure 10. A comparison between simulated (dashed) and measured (solid) H_θ -plane (xy-plane) radiation patterns as a function of phase configurations. The input phases were configured for in-phase two-port activation (after [13]).

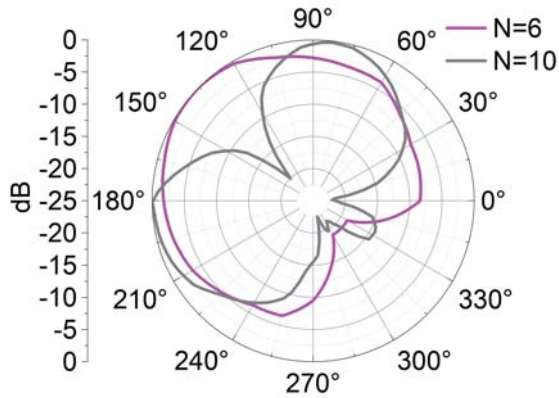

Figure 12. The measured radiation patterns for $N = 6$ and $N = 10$.

topology, demonstrating its capability to steer beams with a 45° step in the azimuthal plane. Additional beamforming configurations, characterized by the presence of notches, were also demonstrated. These are important for applications such as interference suppression and radio localization, thereby showing the versatility of the proposed feed network. This circuit opens the door to a new class of reconfigurable feed networks for conformal arrays, particularly relevant for next-generation reconfigurable front-ends.

5. References

1. G. A. Akpakwu, Bruno J. Silva, G. P. Hancke, and A. M. Abu-Mahfouz, "A Survey on 5G Networks for the Internet of Things: Communication Technologies and Challenges," *IEEE Access*, **6**, 2018, pp. 3619-3647.

2. TE connectivity, "White Paper: Mass Connectivity in the 5G Era," https://www.te.com/usa-en/trends/iot-5g-ai/insights/mass-connectivity-5g-era.html, accessed October 2020.

3. J. G. Andrews, S. Buzzi, W. Choi, S. V. Hanly, A. Lozano, A. C. K. Soong, and J. C. Zhang, "What Will 5G Be?," *IEEE Journal on Selected Areas in Communications*, **32**, 6, June 2014, pp. 1065-1082.

4. W. Roh, J.-Y. Seol, J. Park, B. Lee, J. Lee, Y. Kim, J. Cho, K. Cheun, and F. Aryanfar, "Millimeter-Wave Beamforming as an Enabling Technology for 5G Cellular Communications: Theoretical Feasibility and Prototype Results," *IEEE Communications Magazine*, **52**, 2, February 2014, pp. 106-113.

5. S. Sun, T. S. Rappaport, R. W. Heath, A. Nix, and S. Rangan," MIMO for Millimeter Wave Wireless Communications: Beamforming, Spatial Multiplexing, or Both?," *IEEE Communications Magazine*, **52**, 12, December 2014, pp. 110-121.

6. H. Ren, B. Arigong, M. Zhou, J. Ding, and H. Zhang," A Novel Design of 4 × 4 Butler Matrix with Relatively Flexible Phase Differences," *IEEE Antennas and Wireless Propagation Letters*, **15**, 2016, pp. 1277-1280.

7. L. Zhong, Y. Ban, J. Lian, Q. Yang, J. Guo and Z. Yu, "Miniaturized SIW Multibeam Antenna Array Fed by Dual-Layer 8 × 8 Butler Matrix," *IEEE Antennas and Wireless Propagation Letters*, **16**, 2017, pp. 3018-3021.

8. J. Lian, Y. Ban, Q. Yang, B. Fu, Z. Yu and L. Sun, "Planar Millimeter-Wave 2-D Beam-Scanning Multibeam Array Antenna Fed by Compact SIW Beam-Forming Network," *IEEE Transactions on Antennas and Propagation*, **AP-66**, 3, March 2018, pp. 1299-1310.

9. C.-H. Hsieh, Y.-T. Lin, H.-C. Jhan, and Z.-M. Tsai," Application of a Two-Dimensional Butler Matrix Antenna Array For Tile-Based Beamforming," *IEICE Electronics Express*, **16**, 11, 2019, pp. 1-6.

10. A. Ocera, P. Farinelli, F. Cherubini, P. Mezzanotte, R. Sorrentino, B. Margesin, and F. Giacomozzi," A MEMS-Reconfigurable Power Divider on High Resistivity Silicon Substrate," 2007 IEEE/MTT-S International Microwave Symposium, Honolulu, HI, 2007, pp. 501-504.

11. H. Tae, K. Oh, H. Lee, W. Son and J. Yu, "Reconfigurable 1 × 4 Power Divider with Switched Impedance Matching Circuits," *IEEE Microwave and Wireless Components Letters*, **22**, 2, February 2012, pp. 64-66.

12. H. Fan, X. Liang, J. Geng, L. Liu, and R. Jin, "An N-Way Reconfigurable Power Divider," *IEEE Transactions on Microwave Theory and Techniques*, **65**, 11, November2017, pp. 4122-4137.

13. V. Palazzi, P. Mezzanotte, and L. Roselli, "A Novel Agile Phase-Controlled Beamforming Network Intended for 360° Angular Scanning in MIMO Applications," 2018 IEEE/MTT-S International Microwave Symposium-IMS, Philadelphia, PA, 2018, pp. 624-627.

14. J. Butler, "Beam-Forming Matrix Simplifies Design of Electronically Scanned Antennas," *Electronic Design*, **9**, 8, April 1961, pp. 170-173.

15. Skyworks®, "AS179-92LF: 20 MHz to 4.0 GHz GaAs SPDT Switch," https://www.skyworksinc.com/-media/D73E805A9AC8424980010E10BE76C5DF.pdf.